Oxid Met (2010) 73:95–113
DOI 10.1007/s11085-009-9164-z

ORIGINAL PAPER

Characterization of Sulfur Distribution in Ni-Based Superalloy and Thermal Barrier Coatings After High Temperature Oxidation: A SIMS Analysis

T. Gheno · D. Monceau · D. Oquab · Y. Cadoret

Received: 2 January 2009 / Revised: 1 June 2009 / Published online: 28 July 2009

Abstract Sulfur segregation was characterized by secondary ion mass spectrometry (SIMS) in uncoated single-crystal Ni-based AM1 superalloys with various S contents and on NiPtAl, NiAl and NiPt bondcoats of complete TBC systems. In spite of technical difficulties associated with diffuse sputtered interfaces, an original sample preparation technique and a careful choice of analysis conditions enabled a chemical characterization of S distribution below metal/oxide interfaces. An initial heterogeneous distribution of S in as-received high S (3.2 ppmw) AM1 was measured. After oxidation, a S depletion profile formed, with a slope that depended on the initial bulk S content. GDMS measurements enabled a quantitative distribution of S in oxidized low S (0.14 ppmw) AM1 to be constructed and discussed in relation to equilibrium surface segregation of S on Ni. The quantity of S integrated in the thermally grown oxide (TGO) was estimated and found to be very similar to that measured from depletion found in the metal. Localized S enrichments in Pt-containing coatings are related to a possible beneficial trapping mechanism of Pt on the adherence of oxide scales.

Keywords Oxidation · Sulfur segregation · Metal/oxide interface · Superalloy · TBC · SIMS

Introduction

High temperature materials, such as superalloys or thermal barrier coatings (TBC), gain resistance from high temperature oxidation by forming a compact, continuous

T. Gheno · D. Monceau (✉) · D. Oquab
CIRIMAT, Université de Toulouse, ENSIACET, 31077 Toulouse Cedex 04, France
e-mail: daniel.monceau@ensiacet.fr

Y. Cadoret
SAFRAN, Snecma Villaroche, 77550 Moissy-Cramayel, France

and adherent oxide scale. Sulfur is known to have a deleterious effect on the adherence of this oxide layer, which is a critical feature for the life span of the system. In this context, it is important to understand S effect mechanisms. To do so, analysis techniques adapted to the localization of S in the system, before and after thermal cycling, are needed. This paper reviews various aspects of S segregation in high temperature metallic alloys, as well as strategies to prevent it. Then, experimental work is presented, which explores the capabilities of secondary ion mass spectrometry (SIMS) to provide a better understanding of S segregation in superalloys and TBC systems. The use of SIMS is not much developed yet in this context, but this technique presents features of great interest. In particular, it is very sensitive, from the ppm to the ppb depending on materials and analysis conditions, i.e., much more sensitive than electron dispersive spectroscopy, electron microprobe or Auger. Moreover, SIMS enables volume analysis with three different modes: depth profiling, 2D and 3D mapping with 0.1 μm lateral spatial resolution which is not possible with impurity quantitative techniques such as glow discharge mass spectroscopy (GDMS) or inductively coupled plasma spectrometry (ICP). Drawbacks and limitations of SIMS for segregation studies are also reviewed.

Sulfur Segregation and its Role on Oxide Layer Adherence

Origin of Sulfur

Sulfur is present in superalloys, as an impurity in raw materials and at each step of the alloy processing. Moreover, in the case of NiPtAl bondcoats, the Pt electroplating and aluminizing equipment are other sources of S contamination [1–3]. So is the grit blasting of the superalloy prior to the coating: the presence of S has been observed on the surface of small oxide particles located at the internal/external bondcoat interface [1]. In a similar observation [4], the oxide particles were identified as alumina. Finally, any sample handling can be a source of contamination.

Theoretical Aspects of Sulfur Segregation

Sulfur strongly segregates to metal free surfaces and to metal/oxide interfaces. Different kinds of segregation can be distinguished. The free energy of equilibrium segregation to surfaces and grain boundaries is generally composed of two contributions: a decrease in surface or interface energy by saturation of free bonds and a decrease in elastic energy by release of stresses in the lattice caused by dissolved atoms [5]. In the case of surface segregation in thermodynamic equilibrium, only the surface atomic monolayer has a different content from the bulk. According to Smialek et al. [6], the S surface coverage on superalloys containing a few ppm of S follows the Langmuir–McLean isotherm (above 800 °C):

$$\theta/(1-\theta) = a \cdot C_s/(1-C_s) \cdot \exp(Q_s/RT) \quad (1)$$

where θ is the surface coverage relative to saturation, C_s is the bulk S concentration, a is a constant, and Q_s is the enthalpy of segregation. Concerning S interfacial

segregation, some features were observed experimentally in the case of oxidized alumina scale forming alloys. It has been found that S segregation is influenced by the interface microstructure and composition, that it is higher at free surfaces (such as interfacial cavities) than at intact metal/oxide interfaces and that it is controlled by the availability of interfacial sites rather than by bulk diffusion [7, 8].

A second type of interfacial segregation can be called "dynamic segregation" [9]. The driving force of dynamic segregation is a gradient of chemical, electrostatic or elastic potential between the bulk and the interface, due to a change in thermodynamic conditions. In the case of metals, the solute–clustering model is based on the diffusion of solute–vacancy bindings towards vacancy sinks such as grain boundaries [10].

Third, the presence of an impurity like S at the oxide/metal interface can also be explained by the phenomenon called "interface sweeping", which is more an accumulation than a segregation. This idea was first suggested in the case of S segregation to a Cr_2O_3/Cr interface formed at 950 °C [11]. According to a more recent study of S distribution in S-rich oxidized β-NiAl alloys [12], it was also suggested that when the oxide scale grows predominantly by oxygen inward diffusion, the interface moves inward and can incorporate S from the alloy. However, in this case, the interface is the place of a chemical reaction, and S is more likely to be integrated in the oxide rather than accumulated at the interface, via the formation of oxysulfide compounds for example. On the contrary, when the oxide growth is controlled by an outward flux of cations, the metal atoms get ionized at the metal/oxide interface and transfer across the interface. In this case S should stay on the metal side. The consequence is the relative enrichment of S induced by the metal depletion.

Location of Sulfur in Oxidized Alloys and Effects of this Segregation

Many authors have experimentally highlighted the detrimental effect of S on the adherence of oxide scales [1, 11, 13–16], be it on Ni or Fe based alumina or chromia scale forming alloys, after isothermal or cyclic oxidation. Smialek et al. [6] have formalized this S-linked oxide scale spalling by identifying a critical S content for maximizing the adherence of alumina on Ni-based superalloys. This value of S_c depends on bulk thickness, but is $\sim$0.2 ppmw for a 1 mm thick superalloy.

Adherence Loss at an Intact Interface

First principle calculations [17] have shown that generally, S segregates to intact Ni/Al_2O_3 interfaces, unless they are Al-rich. The presence of S impurities segregated at these interfaces, as well as $NiCrAl/Al_2O_3$ ones [18], has a deleterious effect on alumina scale adhesion. Experimental evidence of this presence has been brought by Hou and Stringer [11]. After removal of unspalled oxide scales in vacuum, a S surface coverage of 17–19% was measured by scanning Auger spectroscopy on $FeCrAl/Al_2O_3$ and $NiCr/Cr_2O_3$ systems oxidized between 900 and 1100 °C. Sulfur was found both on interfacial voids and on intact interfacial areas. The analyzed areas are oxide imprints, and segregation could only have happened before the separation. Using Auger electron spectroscopy, Tolpygo and Viefhaus [19] also

detected S at an intact FeCrAl/Al_2O_3 interface, with a coverage of 50 at.%. According to these authors, the driving force of this segregation is plastic stress and strain to the interface.

Development of Existing Defects

Grabke et al. [20] disagreed with the weakening of an intact interface by S. According to these authors, S segregates as S^{2-} ions. Size and charge effects prevent it from segregating to an intact metal/oxide interface. In this perspective, the observations of S at intact interfaces could be explained by the presence of small voids or other defects near the interface, these voids being unresolvable by SEM [21]. Then, the explanation of the detrimental role of S is that S segregates to free surfaces of voids and cavities formed beneath the oxide scale. This leads to a decrease in their surface energy, which favors their formation and growth since the critical radius of nucleation is reduced [20]. To summarize, Grabke et al. postulated that S promotes the formation of defects and consequently delaminating of the metal/oxide interface. Hou and Priimak [22] have provided evidence of the effect of S on existing defects in the interfacial region of oxidized NiAl alloys. They inferred that S weakens the interface by accelerating crack propagation between pores, in addition to enhancing pore formation.

Locating Sulfur in TBC Systems

Sulfur location in TBC systems has been studied by Molins et al. [23, 24], using a β-(Ni,Pt)Al coating deposited on an AM1 superalloy substrate with about 2 ppmw S and oxidized at 1100 °C. The chemical characterization was conducted using analytical transmission electron microscopy (STEM-EDX). Sulfur was detected along β/β grain boundaries, in association with topologically close-packed (TCP) particles and α-Cr precipitates in β grains, along γ'/β grain boundaries and at γ'/Al_2O_3 and α-Cr/Al_2O_3 interfaces. Cr was also found to segregate to γ'/β interfaces, and S enrichment was observed at the surface of the Cr precipitates.

Models of the Sulfur Effect

Very few models give details about the S effect in its entirety. Rivoaland et al. [25] developed a model based on observations from oxidized NiAl single-crystals. This model involves S segregation to the Ni-rich surface of transient cavities, formed by vacancy injection during outward growth of transient alumina. These cavities are expected to be subsequently filled by inward growth of alpha-alumina. The oxide adherence is weakened by the presence of trapped S, which also favors the formation of interfacial voids and scale spallation under growth and/or thermal stresses. Haynes et al. [26] also considered the stabilization of voids by S in a model of cavity growth for a high S (7 at. ppm) NiAl coating. If the S concentration increases significantly, one could expect several changes: (i) more voids should appear on grain bodies; (ii) more voids should grow over grain boundaries and these voids could be expected to coalesce and form "trenches"; and (iii) more voids with

either smaller diameter or more shallow depth of penetration into the NiAl should coalesce and form large diameter voids with a relatively shallow depth of penetration into the coating.

Even if the deleterious effect of S on the adherence of oxide scales is not fully explained, it is at least identified and some strategies exist to limit its effect.

Adopted Strategies to Counter the Sulfur Effect

There are three main strategies to limit the detrimental effect of S and these are (1) using a low S material, (2) adding some Pt and (3) doping with "reactive elements" (REs). The use of REs to increase the adherence of oxide scales is widely documented [13, 15, 26–29]. The most commonly used elements are Y, Hf, Zr and their oxides. Doping is realized up to a few hundred ppm. Regardless of the S effect, REs have a positive impact on the adherence of oxide scales. However, this strengthening by segregation of REs to the metal/oxide interface is less important than the weakening caused by S segregation [15]. Until the early 1980s, the proposed mechanisms associated with the RE effect did not take into account the role of S. Funkenbush et al. [13] have proposed a new mechanism: as REs form stable sulfides, they can react with S during liquid phase processing and thereby remove sulfur from the alloy, or in the solid state, thereby producing a refractory sulfide and reducing the concentration of S in solution, which would be available to segregate. If REs are introduced in an oxidized state, they can provide additional metal/oxide interfaces, and reduce the quantity of S which segregates to the critical, protective interface. A reaction between these oxides and sulfur to form oxysulfides is also considered [13]. According to Meier et al. [28], in the hypothesis of S trapping, the efficiency of the RE increases with the thermodynamic stability of the sulfide, in particular if it does not form any more stable carbide, nitride or oxide, in which case it would be itself unavailable. These mechanisms are shared by other authors, such as Smialek [15] and Grabke et al. [20], but they do not have unanimous support. For instance, Pint [27] proposed an opposite mechanism: by segregating to the metal/oxide interface, REs cause the surface energy to increase, reducing the driving force for S segregation. Further, concerning Y for example, the oxide is more stable than the sulfide, so the formation of the sulfide would need both a high S activity and a low oxygen activity. Pint added that the dissolution of RE oxides has already been observed in such systems, followed by the diffusion of the element to the surface. The dissolution is also expected to occur with sulfides, which would be detrimental for the system.

Another strategy is to desulfurize the material before using it, via annealing under hydrogen. The main technique has been proven and formalized by Smialek [15, 30]. It consists in inducing S segregation to the surface of the material by a high temperature annealing under an H_2-bearing, reducing atmosphere. The hydrogen atmosphere suppresses or limits oxidation and evacuates S through the surface as H_2S. Depending on the annealing conditions (time, temperature, sample's thickness), this technique enables one to lower the concentration of S from a typical 10 ppm to less than 0.1 ppm.

Within the aeronautical industry, these two strategies are currently used to reduce the S content of superalloys for TBC systems, since the oxidation behavior of the coating is directly influenced by the S content of the substrate [26, 31, 32]. However, all mechanisms are not elucidated and there are some side effects. For example, annealing under hydrogen leads to a slight decarburization [28, 33] and has an influence on other elements [33]. Besides, there is a synergy between desulfurization, decarburization and RE doping, with Hf for example [29]. Thereby the association of desulfurization and doping is particularly efficient [28].

The third strategy to counter the detrimental S effect consists of introducing Pt in the metal, typically up to 10 wt%. Compared to a non-modified coating, a gain in the adherence of the oxide scale is observed experimentally [2, 26, 34–37]. The β-(Ni,Pt)Al coatings are currently used in the industry and their role in limiting the deleterious effect of S has been proven. Introducing of Pt in bondcoats enables one to eliminate S segregation at the metal/oxide interface [38]. According to Cadoret [39], there is a correlation between S and Pt contents and the life span of the considered system. Experimental studies [40, 41] on NiAl and NiPtAl alloys support the idea that Pt enables to maintain an Al-rich phase near the metal/oxide interface, which is assumed to limit the formation of interfacial transient cavities during the growth of θ-Al_2O_3. In addition, S segregates more to Ni-rich than to Al-rich surfaces [40]. Consequently, the effect of Pt is to reduce both growth of transient cavities and S segregation at the free surface of these cavities. Referring to the Rivoaland et al. [25] model of the S effect, these two consequences are beneficial for the adherence of alumina scales.

This review of S effects and of its interactions with REs and Pt shows that the establishment of active mechanisms can only be supported by a characterization of S distribution at a local scale. This characterization is difficult because of the very low S content in the industrial and desulfurized systems. Recent advances in SIMS analysis, including enhanced spatial resolution, 3D imaging and high mass resolution motivate the use of this technique on complex oxidized systems.

Materials and Experiments

Single crystals of AM1 superalloy, with three different S concentrations, were grown at the SNECMA (France) in the form of cylindrical rods with a cross section of 8 mm after machining. The bulk S content of the samples was measured by GDMS (Shiva Technologies, Toulouse, France). The standard alloy, referred to hereafter as high S (HS) contained 3.2 ppmw S, whereas the S content of the melt-desulfurized versions of the alloy, referred to hereafter as low S 1 and 2 (LS1 and LS2), were measured at 0.41 and 0.14 ppmw, respectively. The AM1 composition is given in Table 1. Prior to oxidation, sample surfaces were mechanically polished to a final grade of 1 μm, and then cleaned ultrasonically first in acetone and then in ethanol. The samples were oxidized in air at 1100 °C for 15 h, developing a 1.5 μm thick oxide scale. Complete TBC systems were also prepared, using a grit-blasted AM1 substrate which contained less than 1 ppmw S. 60 μm thick, single-phase β-NiAlPt

Table 1 Chemical composition of AM1 Ni-based single crystal superalloy (wt%) with three different S bulk concentrations measured by GDMS (ppm in weight)

Cr	Co	Mo	W	Ta	Al	Ti	Ni	S (ppmw)
7.5	6.5	2	5.5	8	5.3	1.2	bal	3.2 (HS)/0.41 (LS1)/0.14 (LS2)

bondcoats were obtained by electroplating 5–8 μm Pt on the substrate, followed by vapour-phase aluminizing at 1100 °C. 60 μm thick, single-phase β-NiAl bondcoats were prepared by vapour phase aluminizing at 1100 °C, whereas γ/γ'-NiPt bondcoats were obtained by electroplating 5–8 μm Pt on the substrate. After annealing, the three coatings were grit-blasted, preoxidized in vacuum and yttria stabilized zirconia (YSZ, ZrO_2-8%Y_2O_3) layers were deposited by electron beam physical vapor deposition (EBPVD). Finally, they underwent cyclic oxidation in air at 1100 °C. Each cycle consisted of 1 h dwell at 1100 °C followed by 15 min cooling down to 80 °C using high pressure air flow. The NiPtAl, NiAl and NiPt coating-base TBC systems were respectively oxidized 168, 127 and 235 cycles.

The SIMS analyses were performed on a CAMECA IMS 4f with 6f-modified electronics, using Cs^+ primary ions and detecting negative secondary ions. The mass resolution was set at $M/\Delta M = 2000$, enabling the separation of ^{32}S and $^{32}O_2$ signals. Indeed, 99.76% of O nuclides have a mass of 15.995 u, whereas 95.02% of S nuclides have a mass of 31.972 u, which gives a theoretical $M/\Delta M$ of 1780. The sputtering rate has been determined using crater depth measurements on AM1 and associated TGO by interferometry. The rates were different in metal and oxide. In the usual conditions (primary current = 100 nA, raster size = 100 μm × 100 μm), the sputtering rates were 11.7 and 3.05 nm/s for the metal and the oxide, respectively. For other conditions, sputtering was assumed to be proportional to the primary current and inversely proportional to the rastered area (checked for other materials before). The same values were used for all the metallic phases, even if the sputtering rate might actually be different for each one. After being oxidized, samples were cut and polished (final grade 1 μm) to provide cross sections, which have been analyzed by ion microprobe imaging. They were also prepared for depth profiling and ion microscope imaging.

The SIMS sputter profiling technique presents drawbacks that can strongly disturb the results. In particular, particles from the sides of the sputtering crater may possibly settle on the bottom of the crater, in the analyzed area. This phenomenon is particularly deleterious when, considering an impurity, the analysis progresses from a rich zone to a poorer one. Then, collected ions might actually come from the rich zone, and the concentration in the poor zone can be overestimated. For this reason, it is always better to observe the appearance of an impurity rather than its disappearance. In the case of interfacial segregation, it is beneficial to realize each profile in both ways, i.e. from the oxidized surface to the bulk (*front-side*) and from the bulk to the surface (*back-side*), in order to avoid artificial tails.

The benefits of back-side SIMS profiles have been related in the field of semiconductors [42], where SIMS analysis is widely used. Back-side SIMS profiling was also used to characterize Y distribution in chromia-forming alloys [43]. In the

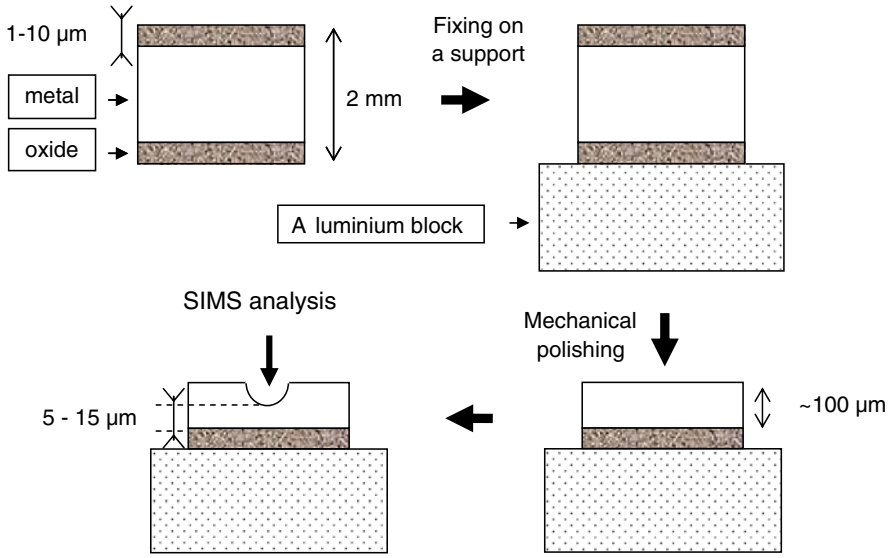

Fig. 1 Sample preparation for back-side SIMS analysis

present study, emphasis was put on back-side profiles applied to S distribution in TBC systems. Indeed, when analyzing a sample by the front (oxidized) side, the surface state is more difficult to refine. This (already high) roughness is amplified during the sputtering, and the depth resolution drops. Back-side SIMS required a specific sample preparation (Fig. 1). Samples were first thinned down by mechanical polishing to about 100 µm. Then, a metallic wheel with an abrasive liquid was used to produce a dimple, so as to leave only 5–15 µm of metal on the oxide. A commercial dimpling machine equipped with a 15 mm diameter wheel was used for this purpose. This preparation technique meets the analysis requirements: the remaining metal thickness is controlled, the sample keeps its mechanical resistance and placing it in the sample-holder of the SIMS is easy, the surface state is controlled and the bottom of the bowl is flat compared to the size of the sputtering area. Even with this preparation, the depth resolution is affected by the interfacial roughness of the samples. In the interfacial region, the SIMS signals come from both metal and oxide phases. As sputter and ionization yields strongly depend on the analyzed phase, interpreting data is not obvious in these areas. Their reliability can be influenced by sputter yield and ionization yield variations. For this reason, emphasis was put on S profiles in the metal before the interface, providing more reliable information.

In addition, knowing the S content in the oxide is essential to better understand S segregation. It requires setting a S concentration reference by using another chemical analysis technique because of the reason mentioned above. A direct and quantitative measure of this content in the thin oxide scale could not be realized as part of this study, since it was technically impossible with the envisaged methods (GDMS, laser ablation/ICP/MS, combustion/X-ray fluorescence). Instead, the S content in a massive stoichiometric alumina sample was measured both by GDMS

and SIMS. The quantitative result of the GDMS measure was associated with the S/O ratio obtained by SIMS. As the O content is approximately the same in stoichiometric alumina and in the oxides formed on the studied materials (Al_2O_3 with some Cr_2O_3 and $NiAl_2O_4$), this S/O ratio has been used as a reference. The S content in the TGOs has been estimated by comparing the S/O ratio in the oxide with this reference. S/O ratios were taken both from back-side and front-side profiles, in order to avoid artifacts. However, the results of these estimates have to be considered with caution. Indeed, since the interfacial roughness has the same order of magnitude than the thickness of the TGO, obtaining steady signals from the thin oxide has not always been possible. In the case of front-side analyses, these estimates have been technically difficult because of the insulating character of alumina.

Results and Discussion

Sulfur Distribution in Unreacted AM1

SIMS analyses were performed on as-received AM1 with 3 different S contents. Depth profiling (Fig. 2) shows 1.5 ± 0.5 μm thick and 2 μm spaced S-rich zones in HS AM1 (3.2 ppmw). Ion microscope imaging allows visualizing this heterogeneous distribution. S-rich zones are well aligned on an axis perpendicular to the surface. Although AM1 is supposed to be a single crystal superalloy, it is possible that these local S enrichments are present at a low-angle grain boundary; further EBSD analysis would be necessary to check this assumption. Nevertheless, it is worth to note that such heterogeneities were not observed on LS samples (0.41 and 0.14 ppmw), and only seldom on the HS one. In order to test the supposed

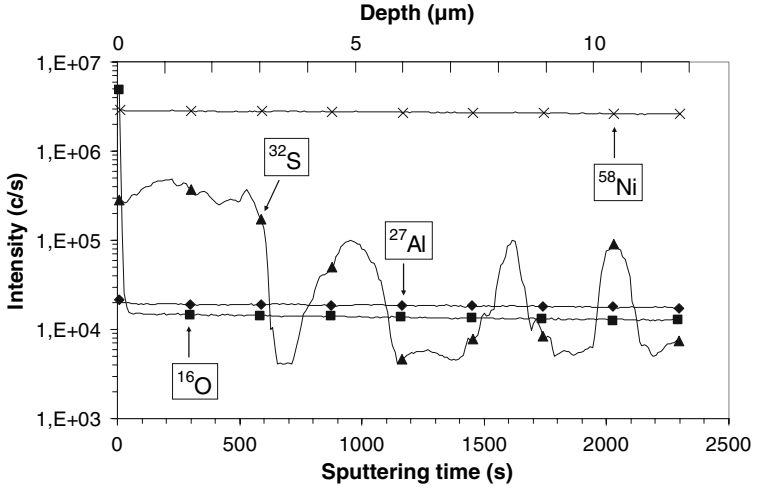

Fig. 2 SIMS depth profiles measured from an as-received (un-oxidized) polished AM1 (S: 3.2 ppmw) surface and showing S-rich zones

proportionality between average S content measured by GDMS and intensity measured by SIMS, normalized S intensities ratios between samples have been calculated and compared to GDMS contents ratios. Normalized intensities are similar for LS samples, and 3.6 times higher for the HS one, instead of 23 times as measured by GDMS. However, SIMS response has to be linear (intensity proportional to concentration) for such low concentrations. Considering these two observations, it seems that samples differ in their bulk S content and in their S-rich zones (number, size). The GDMS probe is 8 mm-wide and it does not allow observing variations which were revealed by SIMS, thanks to a 30 μm-wide analysis area.

Sulfur Distribution in Oxidized AM1

Depth profiling SIMS was carried out on the HS (3.2 ppmw S) and LS2 (0.14 ppmw S) samples, oxidized 15 h at 1100 °C. Figure 3 shows back-side profiles measured on the LS2 sample. These profiles display similar shapes in the case of the HS sample. The logarithmic scale (Fig. 3a) provides an overview of the oxidized samples. In the metal, the S and Al signals decrease gradually through the entire explored depth. This is evidence of a long distance S depletion. Then a sudden increase marks the beginning of the interfacial region and the S signal stays relatively high in the oxide. This is likely due to an integration of S in the oxide as mentioned in the review. However, as SIMS intensity strongly depends on the ionization yield, S intensity variations can not be directly interpreted in terms of concentration variations in the case of a multiphase material. The S content in the oxide was therefore estimated according to the method described earlier. Average contents of 0.8 ppmw for the LS2 sample and 9 ppmw for the HS were obtained in the oxide scales. The linear scale (Fig. 3b) shows a S peak prior to the maximum of O and Al signals. This is likely to result from S segregation or accumulation at the interface. Figure 4 presents S depletion profiles in the bulk of HS and LS2 back-thinned samples and enables to highlight the effect of initial bulk S level on S interfacial segregation. The experimental conditions were not exactly the same for all the analyses. However, this leads to very small variations of the sputtering rate (<4%), therefore the profiles were not significantly disturbed. Offsets were added to distinguish the curves. Figure 4 clearly shows that the S depletion slope depends on the initial S content in the sample.

Discussion of S Segregation Mechanisms in the Case of Low S (0.14 ppmw) Oxidized AM1

In order to better understand S distribution in low S oxidized AM1, quantitative estimates have been made from experimental profiles corresponding to the LS2 sample. It was found that:

(i) the quantity of S corresponding to the S depletion measured by SIMS in the metal under the oxide scale is similar to the theoretical quantity of S which would segregate at the free surface of a Ni sample under the same thermal treatment

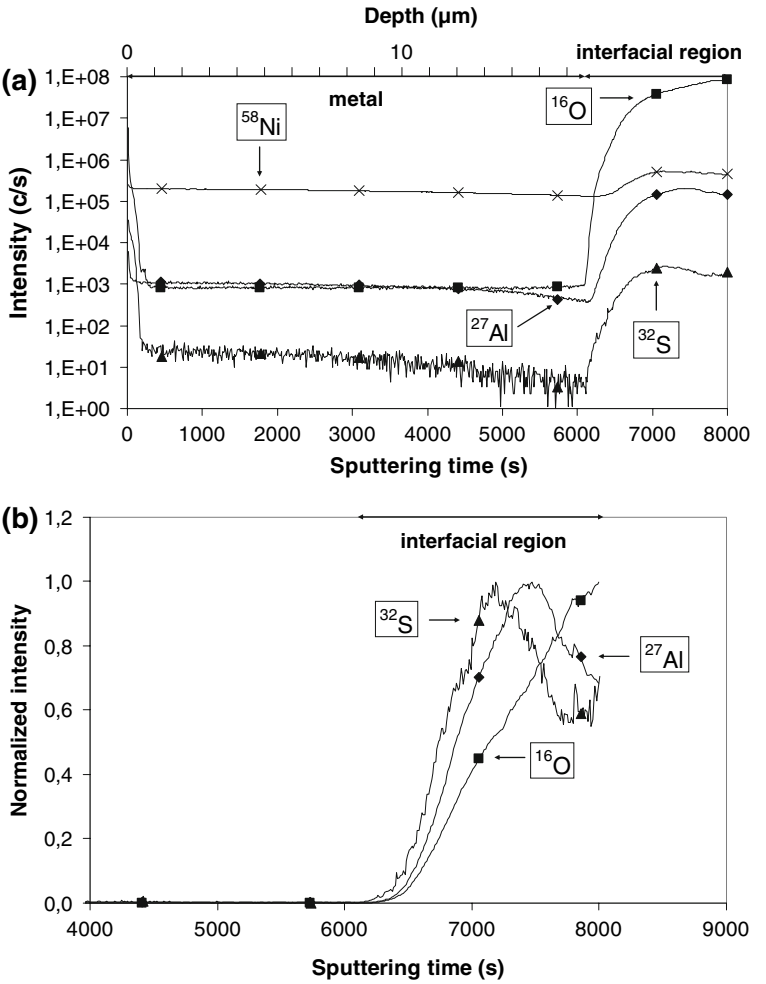

Fig. 3 SIMS depth profiles measured from the back side of oxidized (15 h at 1100 °C) low sulfur AM1 (S: 0.14 ppmw), **a** logarithmic scale, **b** linear scale—intensities have been normalized with respect to the maximum for each element

(15 h at 1100 °C). In other words, the measured depletion corresponds to 1.7×10^{-11} mol/cm^2. If this quantity was gathered at the interface, the surface coverage fraction would be 6.7×10^{-3}. In comparison, the surface coverage expected from the Langmuir–McLean isotherm is 6.9×10^{-3} in the conditions of this study, for S at the surface of pure Ni (the value is calculated from data in [6]).

(ii) In the eventuality that S segregates to the metal/oxide interface with the previously estimated coverage, sputtering the interfacial layer during a SIMS analysis should cause a peak with an amplitude of about 500 times the base level. This value is consistent with the experimental profiles, as represented in Fig. 3, which show an increase of 2–3 orders of magnitude for the S signal when the interface is crossed.

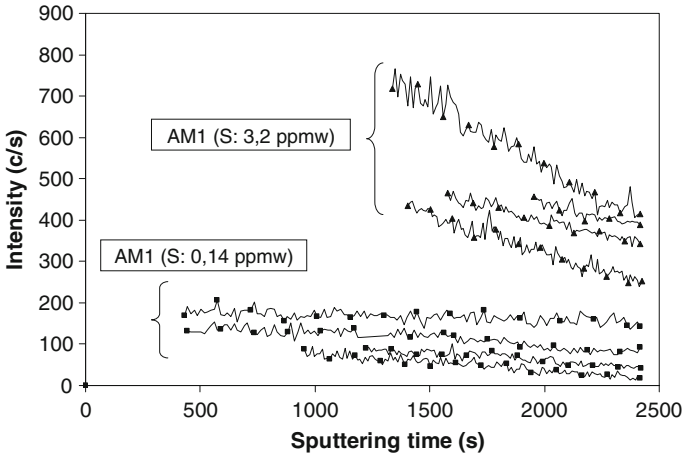

Fig. 4 Sulfur SIMS depth profiles in bulk alloy, linear scale with offsets, measured from the back side of oxidized (15 h at 1100 °C) AM1 samples (S: 0.14 and 3.2 ppm), just below the metal/oxide interface

(iii) The quantity of S integrated in the oxide scale was estimated at 1.2×10^{-11} mol/cm^2, which is very similar to the S depletion measured in the metal.

In the case of HS AM1, the quantity of S corresponding to the measured depletion could not be estimated because of the heterogeneous distribution of S. After normalization (either to Ni or Al SIMS intensities), S interfacial peaks are one order of magnitude higher for the HS sample than for the LS2 one. Besides, the S concentration in the oxide scale is about 10 times higher for the HS sample and corresponds to 1.1×10^{-10} mol/cm^2.

These results show that the quantities of S which are accumulated at the interface and in the oxide scale depend on the initial S content. According to these estimates, it seems that a thermal treatment of 15 h at 1100 °C on AM1 with 0.14 ppmw S is able to generate an interfacial S concentration which is similar to the one expected from the Langmuir–McLean isotherm in the case of S segregation at the surface of pure Ni. Above all, the experimental peaks at the interface and the S signals in the oxide scale are consistent with the measured depletion. This work shows that S has been distributed from the metal to the interface and the oxide scale, but it does not enable the establishment of a fully quantitative S balance.

With better quantification of the S interfacial coverage, using techniques such as scratch test and scanning Auger microscopy [11], a more complete S mass balance could be realized. Its combination with the present back-side SIMS method could enable one to elucidate the details of sulfur segregation in low S alloys.

Study of Sulfur Distribution in "Commercial" TBC After Thermal Cycling in Air

SEM-EDS analyses have been realized on cross sections of the three coatings in order to determine their microstructure below the metal/oxide interface after thermal cycling at 1100 °C. Phase transformations occurred in the three coatings

and Table 2 gives the chemical composition of the first phase below the interface for each coating.

Ion microprobe imaging was realized on a cross section of an oxidized (168 1 h-cycles at 1100 °C) AM1 + NiPtAl + YSZ sample. Figure 5 shows O, Al, S and Pt maps and reveals the presence of S near grit blasting alumina particles. This observation was confirmed and completed by back-thinned sputter profiles presented on Fig. 6a. The first increase of O and Al signals marks the presence of grit blasting alumina 29 μm away from the metal/oxide interface. Both signals stay high for a longer time than the corresponding thickness of the alumina particles. This is due to an analysis artifact (particles settlement from the crater's sides to the analyzed area). Figure 6b shows the presence of a 2.2 μm-thick undetermined oxide in contact with grit blasting alumina. A S enrichment (0.5 μm-deep peaks) is also visible 3.2 μm before this oxide and during the sputtering of grit blasting alumina. As mentioned earlier, this enrichment was already observed [1, 4] and might be the result of a contamination induced by the grit blasting. According to the S/O ratio and using the GDMS calibration, the S content can be estimated to about 300 ppmw inside or near the alumina grit from the blasting.

On the same sample, depth profiles were performed closer to the interface, in order to avoid the sputtering of the grit-blasting alumina, which is deleterious to the rest of the analysis. To do so, the samples were polished closer to the interface before the SIMS analysis. These back-side depth profiles (Fig. 7a) clearly show S-rich areas 7 μm before the interface. As the sputtering starts where the sample preparation has been stopped, this depth of 7 μm is a lower limit. This enrichment is located in 200–650 nm-thick zones and presents amplitude of 100–1000 times the base level. Around the S-rich areas, this base level is 10 times lower than in the bulk of non-oxidized AM1. In addition, the base level stays particularly low in the interfacial region, in opposition to the behavior of the S signal in oxidized bare AM1, but it strongly increases within the oxide scale. According to the S/O ratio, the S content is about 3 ppmw in the TGO.

Back-side ion microscope images were obtained starting at a distance of 4.5 μm before the interface; they illustrate the S enrichment recorded in the profile of Fig. 7a. The images, represented in Fig. 7b, were recorded at a distance comprised

Table 2 Chemical composition (SEM-EDX) of the major phase below the metal/oxide interface of three bondcoats (NiPtAl, NiAl, NiPt) after thermal cycling in air at 1100 °C

Sample coating	NiPtAl	NiAl	NiPt
Major phase below the metal/oxide interface (thickness)	β (20 μm)	γ' (3–6 μm)	γ (10 μm)
Chemical composition (at.%)			
Ni	49.3	64.4	60.4
Al	29.5	18.6	6.2
Pt	8.6	0.0	5.6
Cr	6.2	4.5	13.1
Co	4.2	5.6	7.8

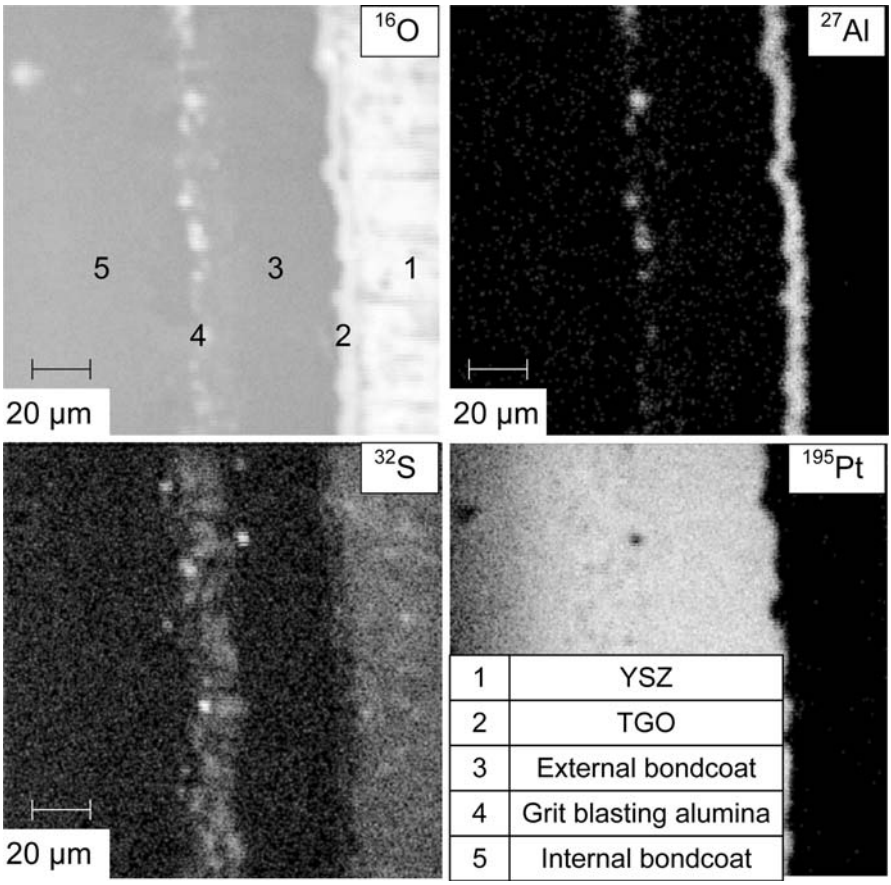

Fig. 5 SIMS image (microprobe mode) of an oxidized AM1 + (Ni,Pt)Al + YSZ system (168 1 h-cycles at 1100 °C), cross section, intensities converted to grey levels with a logarithmic scale

between 4 and 2.8 μm from the interface. The interval between each consecutive image is 200 nm. During the sputtering, S-rich zones (lateral size: 100 nm to 10 μm) appear and disappear in the analyzed area. O and Al maps were also recorded during this experiment. O distribution also presents rich zones, appearing and disappearing, but no correlation exists between O and S signals. In a recent work [23, 24], S was found to co-segregate with Cr in NiPtAl coatings. Here, no correlation was found between S and Cr or any other element, even when detecting positive secondary ions. Field emission gun scanning electron microscopy (FEG-SEM) was also carried out, but S-rich zones could not be identified. This is certainly due to the nanometric size of the enriched areas as described with STEM-EDX [23, 24].

Unlike NiPtAl, the NiAl coating did not show any S enrichment in the metal before the interface. S distribution in NiAl (Fig. 8) is very similar to that of uncoated AM1.

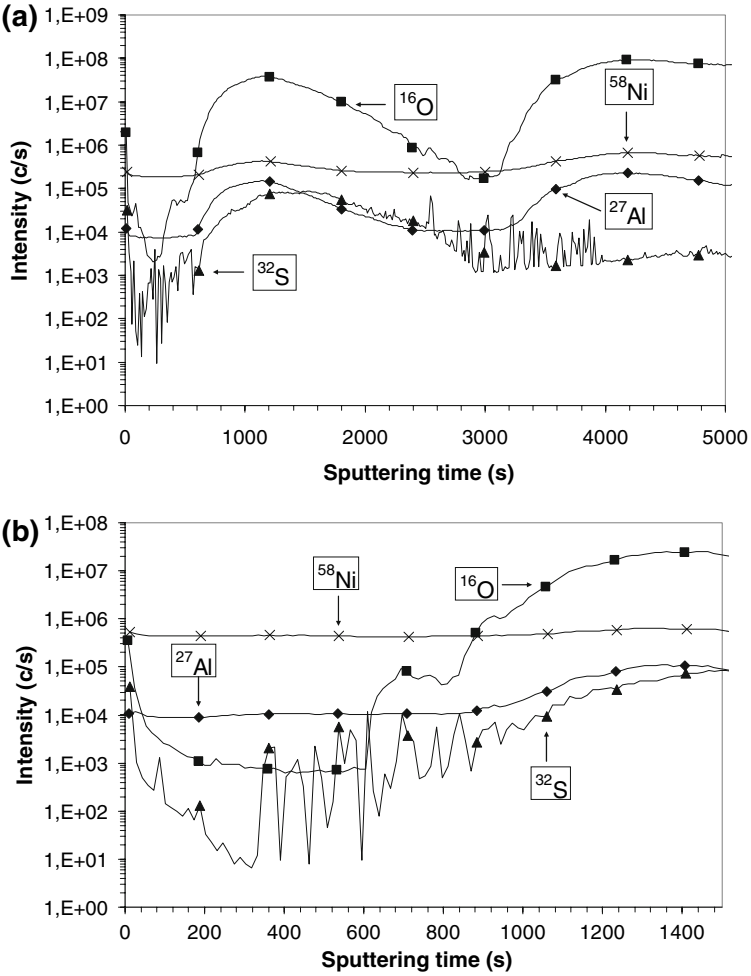

Fig. 6 SIMS depth profiles measured from the back side of oxidized (Ni,Pt)Al coating (168 1 h-cycles at 1100 °C), **a** grit blasting alumina particle 29 μm below the metal/oxide interface, **b** S enrichment near an undetermined oxide particle next to a grit alumina particle about 30 μm below the metal/oxide interface

S signal presents a gradual depletion in the metal, increases at the interface with an amplitude similar to the case of LS2 (0.14 ppmw) AM1 and stays high in the oxide scale. The S content in the TGO is estimated at 2 ppmw.

In the case of γ/γ' NiPt coating, back-side profiles showed S-rich zones in the metal before the interface, but this enrichment is less important than in NiPtAl. The peaks are more spaced out, their amplitude rarely exceeds 500 times the base level and in most cases they are limited to 8 μm before the interface (Fig. 9). In the interfacial region, S signal is relatively high in comparison to the other samples, but it is more likely to result from a strong integration in the oxide rather than from interface segregation. Indeed, S concentration in the TGO is estimated to be more than 300 ppmw, using the S/O ratio. This very high content could be explained by a

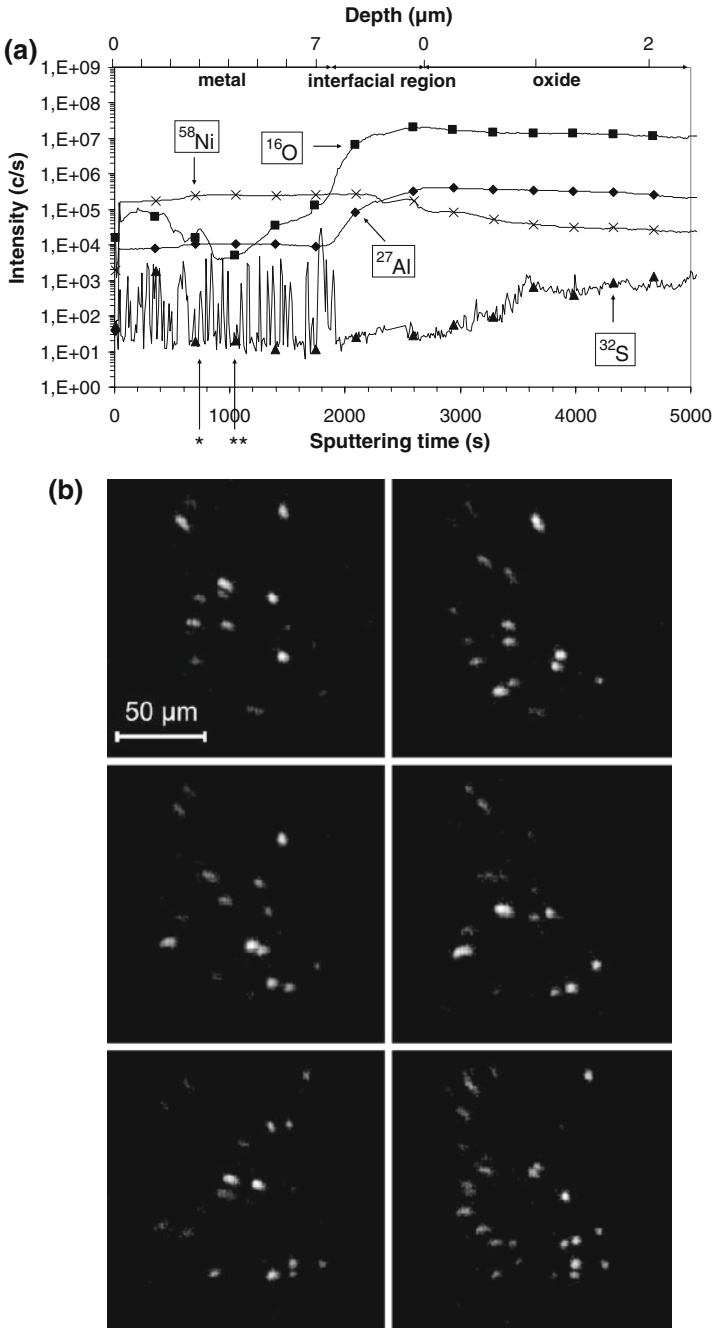

Fig. 7 S distribution in (Ni,Pt)Al coating (after 168 1 h-cycles at 1100 °C), **a** SIMS depth profiles, logarithmic scale, **b** consecutive 200 nm-spaced SIMS images (ion microscope mode), intensity converted to grey levels with a logarithmic scale. The position of this sequence is indicated in **a**, * and ** marking the beginning and the end of the sequence

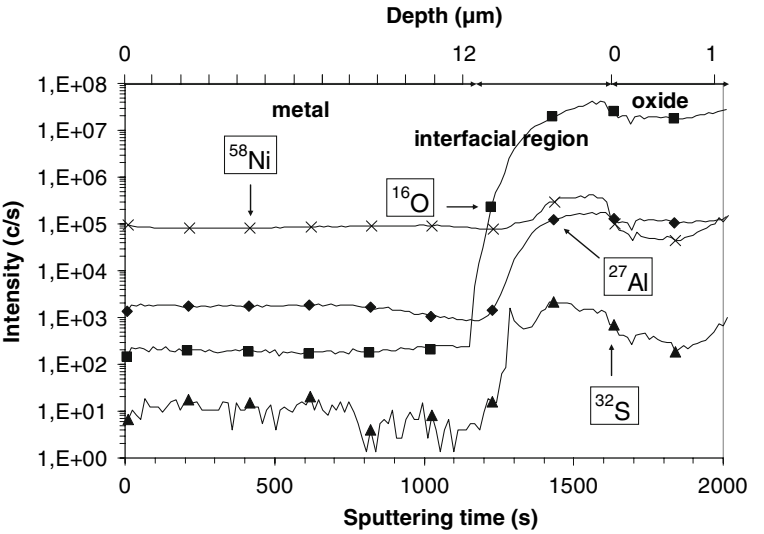

Fig. 8 SIMS depth profiles measured from the back side of oxidized NiAl coating (127 1 h-cycles at 1100 °C), logarithmic scale

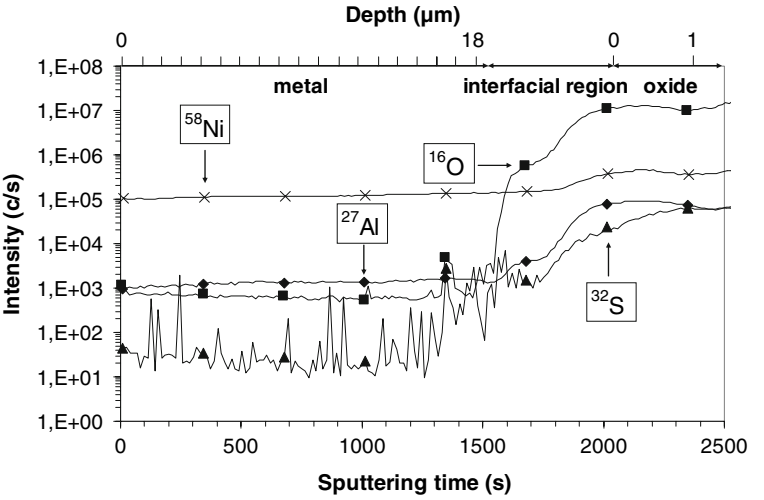

Fig. 9 SIMS depth profiles measured from the back side of oxidized NiPt coating (235 1 h-cycles at 1100 °C), logarithmic scale

difference in the oxidation mechanism between NiPt and the other materials studied here, and this would require further analyses of the TGO.

It was shown that S-rich zones were found in the two coatings containing Pt but not in the NiAl coating. This suggests that Pt plays a role in S segregation, as it seems to offer internal segregation sites that prevent detrimental interfacial segregation. The nature of these sites has not been determined in this study. The

effect of this enrichment might be to trap S in the metal, and as a consequence to limit the critical presence of S at the main metal/oxide interface. In this perspective, the results of this work are in agreement with the positive role of Pt for the TGO adherence as it is presented in the literature review [2, 27, 35–41]. However, this work did not enabled an exact quantification of the amount of S at the metal/oxide interface. Qualitatively, the absence of S at the alloy/TGO interface has been clearly evidenced in the case of NiPtAl, but not in the case of NiPt.

Conclusions

SIMS profiles and images have been conducted on single-crystal Ni-based AM1 superalloys, and commercial TBC systems. The sample back-side preparation enabled a decent chemical characterization of S distribution in the different oxidized alloys, under the metal/oxide interface. Before being oxidized, AM1 superalloy with 3.2 ppmw S had an inhomogeneous S distribution. Depth profiles showed 1.5 ± 0.5 μm thick, 2 μm spaced S-rich zones, while ion microscope imaging revealed that they were well aligned on an axis perpendicular to the surface. After 15 h in air at 1100 °C, back-side profiles provided evidence of extensive S depletion below the AM1/TGO interface, whose slope depends on the initial bulk S content. In the case of low S AM1 (0.14 ppmw), quantitative estimates showed that the experimental peaks at the interface and the S concentration in the oxide scale were both consistent with the measured depletion. With the help of a direct quantification of S interfacial coverage, this approach (back-side and front-side analyses) could provide a complete characterization of S segregation in low S superalloys.

Concerning commercial TBC systems, a comparison was made of the S distribution in NiPtAl, NiAl and NiPt coatings after thermal cycling in air at 1100 °C. Back-side profiles and ion microscope images revealed the presence of S-rich zones in about 10 μm before the metal/oxide interface of Pt-containing coatings. This enrichment could be associated with the positive role of Pt for the TGO adherence.

Acknowledgments The authors are grateful to Claude Armand and Françoise Voillot at the Institut National des Sciences Appliquées, Toulouse, France for conducting the SIMS analyses. The financial support of SNECMA-SAFRAN company is also acknowledged.

References

1. W. Y. Lee, Y. Zhang, I. G. Wright, B. A. Pint, and P. K. Liaw, *Metallurgical and Materials Transactions* **29A**, 841 (1998).
2. Y. Zhang, W. Y. Lee, J. A. Haynes, I. G. Wright, B. A. Pint, K. M. Cooley, and P. K. Liaw, *Metallurgical and Materials Transactions* **30A**, 2687 (1999).
3. J. A. Haynes, *Scripta Materialia* **44**, 1147 (2001).
4. I. Rouzou, R. Molins, and F. Jomard, *Materials Science Forum* **461–464**, 101 (2004).
5. H. J. Grabke, G. Kurbatov, and H. J. Schmutzler, *Oxidation of Metals* **43**, 97 (1995).
6. J. L. Smialek, D. T. Jayne, J. C. Schaeffer, and W. H. Murphy, *Thin Solid Films* **253**, 285 (1994).
7. P. Y. Hou, *Journal of Materials Science Letters* **19**, 577 (2000).

8. P. Y. Hou, K. Prüßner, D. H. Fairbrother, J. G. Roberts, and K. B. Alexander, *Scripta Materialia* **40**, 241 (1999).
9. D. Monceau, *Modélisation des phénomènes de « ségrégation dynamique » dans les céramiques*. PhD Thesis at the Paris 13 University (1992).
10. X. Huang, M. C. Chaturvedi, N. L. Richards, and J. Jackman, *Acta Materialia* **45**, 3095 (1997).
11. P. Y. Hou and J. Stringer, *Oxidation of Metals* **38**, 323 (1992).
12. R. Molins, I. Rouzou, and P. Hou, *Materials Science and Engineering A* **454–455**, 80 (2007).
13. A. W. Funkenbusch, J. G. Smeggil, and N. S. Bornstein, *Metallurgical Transactions A* **16**, 1164 (1985).
14. J. G. Smeggil, A. W. Funkenbusch, and N. S. Bornstein, *Metallurgical Transactions A* **17**, 923 (1986).
15. J. L. Smialek, *Metallurgical Transactions A* **18**, 164 (1987).
16. N. S. Bornstein, M. A. DeCrescente, and J. G. Smeggil, *Materials Science and Engineering A* **120–121**, 175 (1989).
17. W. Zhang, J. R. Smith, X.-G. Wang, and A. G. Evans, *Physical Review B* **67**, 245414 (2003).
18. S. Y. Hong, A. B. Anderson, and J. L. Smialek, *Surface Science* **230**, 175 (1990).
19. V. K. Tolpygo and H. Viefhaus, *Oxidation of Metals* **52**, 1 (1999).
20. H. J. Grabke, D. Wiemer, and H. Viefhaus, *Applied Surface Science* **47**, 243 (1991).
21. H. J. Grabke, G. Kurbatov, and H. J. Schmutzler, *Oxidation of Metals* **43**, 97 (1995).
22. P. Y. Hou and K. Priimak, *Oxidation of Metals* **63**, 113 (2005).
23. R. Molins, I. Rouzou, and P. Hou, *Oxidation of Metals* **65**, 263 (2006).
24. R. Molins and P. Y. Hou, *Surface & Coatings Technology* **201**, 3841 (2006).
25. L. Rivoaland, V. Maurice, P. Josso, M.-P. Bacos, and P. Marcus, *Oxidation of Metals* **60**, 159 (2003).
26. J. A. Haynes, B. A. Pint, K. L. More, Y. Zhang, and I. G. Wright, *Oxidation of Metals* **58**, 513 (2002).
27. B. A. Pint, *Oxidation of Metals* **45**, 1 (1996).
28. G. H. Meier, F. S. Pettit, and J. L. Smialek, *Materials and Corrosion* **46**, 232 (1995).
29. J. L. Smialek and B. A. Pint, *Materials Science Forum* **369–372**, 459 (2001).
30. J. L. Smialek, *Metallurgical Transactions A* **22**, 739 (1991).
31. Y. Zhang, B. A. Pint, J. A. Haynes, and I. G. Wright, *Surface & Coatings Technology* **200**, 1259 (2005).
32. J. A. Haynes, B. A. Pint, Y. Zhang, and I. G. Wright, *Surface & Coatings Technology* **202**, 730 (2007).
33. J. L. Smialek, *Oxidation of Metals* **55**, 75 (2001).
34. Y. Zhang, J. A. Haynes, W. Y. Lee, I. G. Wright, B. A. Pint, K. M. Cooley, and P. K. Liaw, *Metallurgical and Materials Transactions* **32A**, 1727 (2001).
35. P. Y. Hou and V. K. Tolpygo, *Surface & Coatings Technology* **202**, 623 (2007).
36. B. A. Pint, J. A. Haynes, J. H. Schneidel, I. G. Wright, and Y. Zhang. Role of precious metals in high temperature bond coatings, oral communication. *Toulouse's Workshop on High Temperature Corrosion and Protection for Aeronautic Applications, CIRIMAT, 16th May 2008.*
37. B. Gleeson, Advancements in the development of modified γ-Ni + γ'-Ni3Al bond coatings, oral communication. *Toulouse's Workshop on High Temperature Corrosion and Protection for Aeronautic Applications, CIRIMAT, 16th May 2008.*
38. P. Y. Hou and K. F. McCarty, *Scripta Materialia* **54**, 937 (2006).
39. Y. Cadoret and A. Raffaitin, Development of high temperature coatings and TBC bond coats, Oral communication. *Toulouse's Workshop on High Temperature Corrosion and Protection for Aeronautic Applications, CIRIMAT, 16th May 2008.*
40. Y. Cadoret, M.-P. Bacos, P. Josso, V. Maurice, P. Marcus, and S. Zanna, *Materials Science Forum* **461–464**, 247 (2004).
41. Y. Cadoret, D. Monceau, M.-P. Bacos, P. Josso, V. Maurice, and P. Marcus, *Oxidation of Metals* **64**, 185 (2005).
42. Z. X. Jiang, K. Kim, J. Lerma, D. Sieloff, H. Tseng, R. I. Hegde, T. Y. Luo, J. Y. Yang, D. H. Triyoso, and P. J. Tobin, *Applied Surface Science* **252**, 7172 (2006).
43. P. Y. Hou, V. Chia and I. Brown, *Surface and Coatings Technology* **51**, 73 (1992).